Inorganic Chemistry

Article

pubs.acs.org/IC

Photoinduced Ligand Exchange and Covalent DNA Binding by Two New Dirhodium Bis-Amidato Complexes

Scott J. Burya, Alycia M. Palmer, Judith C. Gallucci, and Claudia Turro*

Department of Chemistry and Biochemistry, The Ohio State University, Columbus, Ohio 43210, United States

Supporting Information

ABSTRACT: Two new dirhodium complexes, the head-to-tail (*H,T*) and head-to-head (*H,H*) isomers of *cis*-$[Rh_2(HNOCCH_3)_2(CH_3CN)_6]^{2+}$, were synthesized, separated, and characterized following the reaction of $Rh_2(HNOCCH_3)_4$ with trimethyloxonium tetrafluoroborate in CH_3CN. The products were characterized by ^1H NMR spectroscopy, mass spectrometry, elemental analysis, and single crystal X-ray diffraction. Each bis-amidato isomer has a total of six CH_3CN ligands, two along the internuclear Rh−Rh axis, CH_3CN_{ax}, two in equatorial positions *trans* to the oxygen atoms of the bridging amidato groups, $CH_3CN_{eq}^{O}$, and two in equatorial positions *trans* to the amidato nitrogen atoms, $CH_3CN_{eq}^{N}$. When aqueous solutions of the complexes are irradiated with low energy light ($\lambda_{irr} \geq 495$ nm, 60 min), both types of CH_3CN_{eq} ligands undergo efficient ligand exchange with solvent H_2O molecules to form monoaqua, followed by bis-aqua, adducts, releasing two CH_3CN_{eq} ligands in the process. The quantum yields, Φ_{400nm}, for the *H,T* and *H,H* isomers to form monoaqua adducts are 0.43 and 0.38, respectively, which are substantially greater than the 0.13 yield observed for *cis*-$[Rh_2(O_2CCH_3)_2(CH_3CN)_6]^{2+}$; importantly, no ligand exchange is observed when the complexes are kept in the dark. Finally, low energy excitation ($\lambda_{irr} \geq 610$ nm, 30 min) of the *H,T* isomer was shown to generate photoproducts that covalently bind to linearized DNA, making **2** a potential agent for photochemotherapy that does not require the formation of $^1O_2$, as is typical of organic photodynamic therapy (PDT) agents.

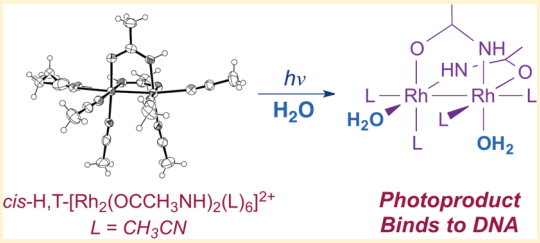

INTRODUCTION

The anticancer properties of cisplatin, *cis*-$Pt(NH_3)_2Cl_2$, were serendipitously discovered by Rosenberg in 1965, and the drug received approval for use in testicular and ovarian cancers in 1978.[1] Cisplatin, which is indiscriminately taken up by cancerous and other rapidly dividing cells, undergoes thermal ligand exchange *in vivo* resulting in the formation of the biologically active species *cis*-$[Pt(NH_3)_2Cl(OH_2)]^+$ and *cis*-$[Pt(NH_3)_2(OH_2)_2]^{2+}$.[2] These active species form intrastrand DNA cross-links that are supported by covalent bonds with the platinum center, where 1,2-GpG lesions represent the major adduct.[2] The resulting platinated DNA, *cis*-$[Pt(NH_3)_2\{d(GpG)\}]$, exhibits a bend of up to 60° to accommodate the Pt bite angle, creating a deformity that is recognized by proteins in the cell, resulting in inhibition of transcription and DNA replication, as well as initiation of cell-cycle arrest and apoptosis.[2]

Of the 23 platinum-based drugs that entered clinical trials following the approval of cisplatin, only carboplatin and oxaliplatin have gained international marketing approval, and nedaplatin, lobaplatin, and heptaplatin have regional approval.[3] Promising third generation complexes, including satraplatin, picoplatin, and triplatin, have failed to outperform the three approved Pt drugs, and complexes with novel mechanisms of action are now being sought.[3,4] Nonplatinum transition metal complexes, including $Rh_2(O_2CCH_3)_4$ (**1**) and $Rh_2(HNOCCH_3)_4$ (**2**), whose structures are shown in Figure 1, also bind covalently to biomolecules through metal coordination,[5] and

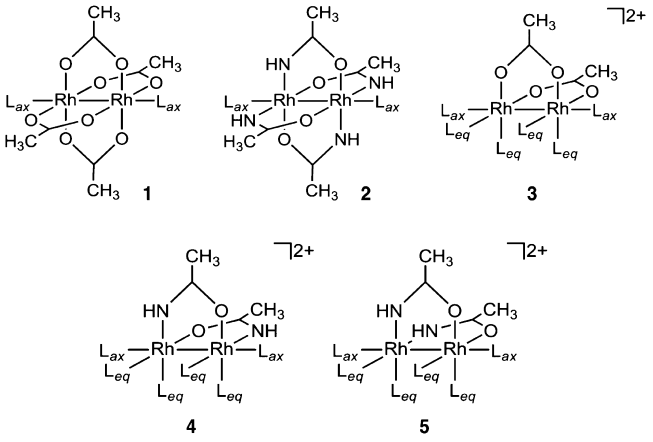

Figure 1. Molecular structures of selected dirhodium complexes; L_{ax} and L_{eq} represent ligand L at axial and equatorial coordination sites, respectively.

these and related complexes have been shown to exhibit anticancer properties, along with *in vitro* and *in vivo* activity.[6,7] However, platinum drugs and other thermally activated complexes, such as the dirhodium systems, also compromise other types of rapidly dividing cells, resulting in severe side effects.[8]

Received: August 15, 2012
Published: October 25, 2012

Photodynamic therapy (PDT) utilizes light to activate drugs in order to achieve spatiotemporal selectivity for cancerous tissue, thus reducing the systemic toxicity to healthy cells.[9] PDT has recently emerged as an alternative, and in some cases a superior approach, to conventional dermatology therapies and for the treatment of endoscopically accessible tumors.[10] The PDT agents undergoing clinical trials or approved for clinical use to date have been organic molecules that sensitize the production of singlet oxygen, $^1O_2$, a reactive oxygen species (ROS) that can effect direct cell damage, vascular shutdown, and activation of immune response.[11] These organic photosensitizers are activated with light in the 600−850 nm range, the PDT window, and systemic toxicity is avoided because the cytotoxic activity is confined to the irradiated tissue.[12] However, these compounds are not operative in the absence of oxygen, which represents a disadvantage in achieving cell death in hypoxic tumors.[13]

Transition metal complexes have also been investigated for use in PDT, and various compounds that sensitize cytotoxic $^1O_2$ upon excitation with visible light have been discovered.[14−19] Additionally, photoactive inorganic complexes with O_2-independent biological activity have been sought,[20] as these would be effective in the hypoxic tissues prevalent in solid tumors.[13,21] Photoactivated cisplatin analogs, one class of photochemotherapy agents that do not require O_2 for activity. These complexes exchange ligands for solvent H_2O molecules only upon irradiation with visible light, and the resulting species covalently bind to double-stranded DNA.[22−24] Moreover, biologically active ligands, in the form of inactive pro-drugs when bound to the metal, can be released photochemically.[25] Because the mechanism of action of these new systems differs markedly from that of traditional PDT drugs, they can potentially lead to important advances in the field.

The irradiation of *cis*-$[Rh_2(O_2CCH_3)_2(CH_3CN)_6]^{2+}$ (**3**, structure shown in Figure 1) with visible light promotes the exchange of two equatorial acetonitrile ligands, CH_3CN_{eq}, for solvent H_2O molecules, and the resulting photoproduct was shown to covalently bind to linearized pUC18 plasmid DNA.[22] Upon irradiation, a 34-fold increase in the toxicity toward Hs-27 human skin fibroblasts was measured for **3**, from IC_{50} = 410 μM in the dark (IC_{50} = concentration required to attain 50% cell death), to IC_{50} = 12 μM upon irradiation (t_{irr} = 30 min, λ_{irr} = 400−700 nm). This finding represents a significant improvement over the 5.5-fold increase observed for hematoporphyrin, an active component in the approved PDT drug Photofrin, under similar experimental conditions.[22]

A variety of inorganic complexes, including *trans,trans,trans*-$[Pt(N_3)_2(OH)_2(NH_3)_2]$,[24a] *cis*-$[Ru(bpy)_2(CH_3CN)_2]^{2+}$,[23a] and *cis*-$[Ru(bpy)_2(NH_3)_2]^{2+}$,[23b] have been shown to undergo photoinduced ligand exchange, but to our knowledge, **3** is the only dirhodium system reported to date to exhibit photoinduced DNA binding and increase in toxicity upon irradiation. In the present work, two new dirhodium bis-amidato complexes, *cis-H,T*-$[Rh_2(HNOCCH_3)_2(CH_3CN)_6]^{2+}$ (**4**) and *cis-H,H*-$[Rh_2(HNOCCH_3)_2(CH_3CN)_6]^{2+}$ (**5**), were synthesized and characterized (Figure 1). Dark stability studies, photolysis experiments, and DNA binding assays were conducted to determine whether these bis-amidato complexes exhibit improved thermal stability, quantum yields, and DNA binding characteristics as compared to **3**.

EXPERIMENTAL SECTION

Materials. Ethanol was purchased from Decon Laboratories, diethyl ether and benzene were obtained from Fisher, glacial acetic acid, acetonitrile, dichloromethane, and anhydrous methanol were procured from Mallinckrodt, and CD_3CN, chlorobenzene, and D_2O were purchased from Sigma-Aldrich. All solvents, except for the distilled acetonitrile used for electrochemistry experiments, were used as received. Acetamide (Fisher), rhodium(III) chloride hydrate (Pressure Chemical), electrochemistry-grade tetrabutylammonium hexafluorophosphate (Bu_4NPF_6, Fluka), and trimethyloxonium tetrafluoroborate (Me_3OBF_4, Sigma-Aldrich) were used without further purification. Boric acid, 1 kb DNA ladder in buffered solution, EDTA, ethidium bromide, electrophoresis-grade agarose, gel loading buffer, Tris base, sodium acetate trihydrate, sodium phosphate, and sodium hydroxide were purchased from Sigma-Aldrich and used as received. Water for photolysis and biological experiments was deionized to a resistivity of 18 MΩ-cm using a Barnstead B-pure filter system. pUC19 plasmid DNA was purchased from Bayou Biolabs, QIAprep Spin Miniprep and Gel Extraction Kits were obtained from Qiagen, and the *Sma*I enzyme, REact 4 buffer and 10X gel loading buffer were purchased from Invitrogen Life Technologies. Complexes **1**,[26] **2**,[27] and **3**[28] were prepared by literature procedures and characterized by ^{1}H NMR spectroscopy; the ^{1}H NMR data for **1**−**3** are consistent with the corresponding literature reports, and the ^{1}H NMR spectrum of **3** is shown in Figure S1a.

***cis*-$[Rh_2(HNOCCH_3)_2(CH_3CN)_6][BF_4]_2$.** $Rh_2(HNOCCH_3)_4$ (**2**, 20 mg, 0.04 mmol) was stirred at room temperature in air with trimethyloxonium tetrafluoroborate (Me_3OBF_4, 24 mg, 0.17 mmol) for 3 days in 6 mL of CH_3CN/MeOH (1:1, v:v), at which time an additional 12 mg of Me_3OBF_4 (11 mg, 0.080 mmol) was added and the mixture was then stirred for an additional 3 days. The volume was reduced to ∼3 mL with a stream of air, and a dark red solid precipitated following the addition of 5 mL diethyl ether. The mixture was centrifugated, and the clear supernatant was removed with a pipet and discarded. The remaining solid was washed with ether and CH_2Cl_2 by adding the corresponding solvent, followed by sonication and centrifugation, at which point the supernatant was removed and discarded. The solid was then dissolved in CH_3CN, and the solution was sonicated and centrifugated. The red supernatant containing the product was transferred to a vial. The insoluble precipitate was discarded, and the red supernatant was dried under a stream of air. The resulting red solid, *cis*-$[Rh_2(HNOCCH_3)_2(CH_3CN)_6][BF_4]_2$ (77% total yield), is found in three isomeric forms: two enantiomers of *cis-H,T*-$[Rh_2(HNOCCH_3)_2(CH_3CN)_6][BF_4]_2$ (**4**), and *cis-H,H*-$[Rh_2(HNOCCH_3)_2(CH_3CN)_6][BF_4]_2$ (**5**). An attempt was not made to separate the enantiomers of **4**. The isomeric mixture of **4** and **5** is soluble in CH_3CN, CH_3OH, and H_2O, but insoluble in ether and CH_2Cl_2. Careful characterization was undertaken following the separation and purification of **4** and **5**.

Separation of 4 and 5. Complex **4** is soluble in CH_3CN:CH_2Cl_2 (1:1, v:v), but **5** does not dissolve in this solvent mixture. Therefore, 1:1 CH_3CN:CH_2Cl_2 was added to the isomeric solid mixture, the sample was centrifugated, and the supernatant containing **4** was removed with a pipet to a new vial, while the precipitate, made up predominantly of **5**, remained as a solid. This process was repeated with the remaining precipitate to ensure complete separation. The supernatant that was collected was dried under a stream of air to give **4** as an oily red solid, and its ^{1}H NMR spectrum is shown in Figure S1b. ^{1}H NMR (D_2O, 400 MHz): δ 2.58 (s, 6 H, $CH_3CN_{eq}^{O}$), 2.56 (s, 6 H, $CH_3CN_{eq}^{N}$), 2.08 (s, 6 H, amidato CH_3). Elemental analysis calculated for $Rh_2[(HNOCCH_3)_2(CH_3CN)_4(H_2O)_2][BF_4]_2$: C 20.71%, H 3.48%, and N 12.08%. Found: C 20.53%, H 3.40%, and N 11.87%. ESI-MS m/z = 243.01 corresponding to $[Rh_2(HNOCCH_3)_2(CH_3CN)_4]^{2+}$.

After the complete removal of **4** in the supernatant as described above, the remaining chalky pink solid of **5** was washed with dichloromethane. CH_3CN was added to the solid, the mixture was centrifugated, and the supernatant, which contained **5**, was removed with a pipet to a new vial with any insoluble precipitate discarded. The

dx.doi.org/10.1021/ic3017886 | Inorg. Chem. 2012, 51, 11882−11890

supernatant was dried by blowing air over the solution and the ^{1}H NMR was collected (Figure S1c). ^{1}H NMR (D_2O, 400 MHz): δ 2.61 (s, 6 H, $CH_3CN_{eq}^{O}$), 2.53 (s, 6 H, $CH_3CN_{eq}^{N}$), 2.07 (s, 6 H, amidato CH_3). Elemental analysis calculated for $Rh_2[(HNOCCH_3)_2(CH_3CN)_4(H_2O)_2][BF_4]_2$: C 20.71%, H 3.48%, N 12.08%. Found: C 20.51%, H 3.41%, N 12.26%. ESI-MS m/z = 243.01 corresponding to $[Rh_2(HNOCCH_3)_2(CH_3CN)_4]^{2+}$.

Instrumentation. Electronic absorption measurements were performed on a Hewlett-Packard (HP) diode array spectrophotometer interfaced with a computer running HP 8453 WinSystem software. Cyclic voltammetry experiments were performed in a three-electrode cell with a Pt working electrode, a Pt wire auxiliary electrode, and a saturated Ag/AgCl reference electrode using a BAS CV-50W voltammetric analyzer (version 2.3). Photolysis experiments were performed using a fan-cooled 150 W Xe short arc lamp (USHIO) in a Milliarc lamp housing unit (PTI) powered by a LPS-220 power supply (PTI) equipped with a LPS-221 igniter (PTI). A 10 cm long water cell, placed between the lamp and the sample, was used to absorb infrared irradiation, and the desired wavelength range was attained using bandpass filters (Thorlabs, fwhm ~10 nm) and/or 3 mm thick Schott color glass long-pass filters (CVI Melles Griot). Electrospray ionization mass spectrometry (ESI-MS) data were acquired on a Bruker MicroTOF spectrometer, and ^{1}H NMR spectra were collected using a Bruker 400 MHz DPX-Ultrashield system. Gel electrophoresis was conducted with an EC-105 unit (EC-Apparatus Corporation), and stained gels were imaged using a GelDoc 2000 transilluminator (Bio-Rad Laboratories) and visualized with Quantity One V 4.6.9 software (Bio-Rad Laboratories).

Methods. Positive ion ESI-MS data for samples dissolved in CH_3CN were referenced to a sodium formate internal standard. ^{1}H NMR spectroscopy was performed in CD_3CN or D_2O, spiked with benzene (25 mM) for quantification, and referenced to the residual CHD_2CN or H_2O solvent peaks.[29] Electrochemical measurements were performed on samples dissolved in distilled CH_3CN containing 0.1 M tetrabutylammonium hexafluorophosphate (Bu_4NPF_6) as the supporting electrolyte, and bubbled for 5 min with N_2 prior to each measurement. Cyclic voltammetry data was recorded at a scan rate of 100 mV/s, and after collecting data for each complex ferrocene was added to the samples to serve as an internal standard (+0.42 V vs SCE in CH_3CN).[30] Elemental analysis (C, H, N) was performed on solid samples by Galbraith Laboratories.

Crystals of **4** suitable for single crystal X-ray diffraction were prepared by adding a saturated solution of the complex in CH_3CN (0.25 mL) to a biphasic mixture of diethyl ether (2 mL) layered above CH_2Cl_2 (2 mL) in a 60 cm long glass tube with ~0.4 cm inner diameter. The solution was stored at 0 °C, and crystals were obtained after 1 month. Complex **5** was crystallized by layering a saturated solution of the complex in CH_3CN (0.25 mL) above pure CH_2Cl_2 (2 mL) in a tube of dimensions described above; the solution was kept at room temperature, and crystals were harvested after 2 weeks.

The diffraction data for **4** and **5** was collected using a Nonius Kappa CCD diffractometer (crystallographic details provided in Table S1). All work was conducted at 150 K using an Oxford Cryosystems Cryostream Cooler. φ and ω scans with a frame width of 1.0° were used. Data integration was done with Denzo, and scaling and merging of the data was done with Scalepack.[31] The structures were solved for the Rh atoms by the Patterson method in SHELXS-97.[32] The rest of the non-hydrogen atoms were located by standard Fourier methods. Full-matrix least-squares refinements based on F^2 were performed in SHELXL-97,[33] as incorporated in the WinGX package.[34] Neutral atom scattering factors were used and include terms for anomalous dispersion.[35]

The crystal of **4** for data collection was a dark red chunk that was cut from a cluster. Examination of the diffraction pattern indicated a monoclinic crystal system. The data collection strategy was set up to measure a quadrant of reciprocal space with a redundancy factor of 3.8, which means that 90% of these reflections were measured at least 3.8 times. Merging the data and averaging the symmetry equivalent reflections resulted in an R_{int} value of 0.074. The asymmetric unit contains one Rh complex, two BF_4^- anions, and a solvent molecule of CH_2Cl_2. One of the CH_3CN_{ax} ligands seems to be disordered, and this was modeled with two sites for this ligand: N(7A)−C(13)−C(14A) and N(7B)−C(13)−C(14B), with atom C(13) common to both sites. Only atom C(13) was refined anisotropically. A bond length restraint of 1.54(1) Å was applied to the C(13)−C(14B) bond length during refinement. The hydrogen atoms bonded to the nitrogen atoms were located on a difference electron density map, added to the model at these positions, and fixed. Both N−H groups are involved in hydrogen bonds with fluorine atoms of the BF_4^- counterions. For each methyl group, the hydrogen atoms were added at calculated positions using a riding model with $U(H) = 1.5 \times U_{eq}$(bonded carbon atom). The torsion angle, which defines the orientation of the methyl group about the C−C bond, was refined for all these methyl groups, with the exception of C(14B). The final refinement cycle was based on 5413 intensities, 1 restraint, and 377 variables, and resulted in agreement factors of R1(F) = 0.081 and wR2(F^2) = 0.142. For the subset of data with $I > 2\sigma(I)$, the $R_1(F)$ value is 0.053 for 3971 reflections. The final difference electron density map contains maximum and minimum peak heights of 1.26 and −0.71 e/Å^3.

The crystal of **5** for data collection was a red rod. Examination of the diffraction pattern indicated a trigonal crystal system. The data collection strategy was set up to measure a hemisphere of reciprocal space with a redundancy factor of 3.1. Merging the data and averaging the symmetry equivalent reflections resulted in an R_{int} value of 0.043. The asymmetric unit contains one Rh complex and two BF_4^- anions. The crystal is a merohedral twin, and the twin law, 0 −1 0/−1 0 0/0 0 −1, was applied during the refinement. The minor component of this twin refined to a value of 0.3393(7). The hydrogen atoms bonded to the nitrogen atoms were located on a difference electron density map and added to the model at these positions, and their positions were refined. Both N−H groups are involved in hydrogen bonds with fluorine atoms of the BF_4^- groups. For each methyl group, the hydrogen atoms were added at calculated positions using a riding model with $U(H) = 1.5 \times U_{eq}$(bonded carbon atom). The torsion angle, which defines the orientation of the methyl group about the C−C bond, was refined. The final refinement cycle was based on 6294 intensities, one restraint, and 358 variables and resulted in agreement factors of R1(F) = 0.027 and wR2(F^2) = 0.056. For the subset of data with $I > 2\sigma(I)$, the R1(F) value is 0.025 for 6153 reflections. The final difference electron density map contains maximum and minimum peak heights of 0.46 and −0.50 e/Å^3.

The quantum yields (Φ) for photoinduced ligand exchange were determined for **3**, **4**, and **5** in H_2O by irradiation with 400 and 550 nm light, filtered using appropriate bandpass filters with 10 nm bandwidths.[36] Electronic absorption spectroscopy was used to quantitate the decrease of reactant concentration as a function of irradiation time (moles reacted/s), and ferrioxalate and Reinecke's salt actinometers were used to determine the intensity (Einsteins/s) of the Xe arc lamp at 400 and 550 nm, respectively.[36,37] Due to the low extinction coefficients and low solubility of the complexes, optically dense ($A > 4$) solutions could not be prepared for quantum yield determinations, and a modified actinometer procedure was developed. Actinometry was performed with various concentrations of the two actinometers with absorption matched to the initial absorption of **3**−**5** at the two irradiation wavelengths. A working curve of actinometer absorption versus lamp intensity was then constructed which was used to correlate the absorption of **3**−**5** to the moles of photons absorbed per minute.

For the DNA mobility shift assays, the DNA was linearized by incubating 10 μg of pUC19 plasmid with 50 units *Sma*I in 10 μL REact 4 buffer at 30 °C for 1 h. The mixture was then heated at 65 °C for 10 min to deactivate the enzyme, which was removed from the linearized pUC19 using a QIAquick Gel Extraction Kit. The linearized DNA concentration was determined from the absorption of the DNA bases at 260 nm (ε = 6600 M^{-1} cm^{-1} per base). Samples were prepared in 0.5 mL transparent Eppendorf tubes (20 μL total volume) containing 50 μM linearized pUC19 plasmid, 10 mM sodium phosphate buffer, and the desired concentration of metal complex. Following irradiation or dark incubation, 3 μL of gel loading buffer was added to each tube, and the samples were loaded into the wells of a 0.75% agarose gel in

TBE buffer (Tris-borate/EDTA buffer, 0.09 M Tris-borate, 0.002 M EDTA, pH = 8.0). The gel was submerged in TBE buffer, and gel electrophoresis was carried out at 94 V for 90 min. After the electrophoresis, the gel was submerged in a 0.5 μg/mL aqueous ethidium bromide solution for 30 min, and was then placed in water for 30 min to remove excess dye, followed by imaging.

Density functional theory (DFT) calculations were performed using the Gaussian03 program package and visualized using GaussView 3.0.[38] The B3LYP (Becke, three-parameter, Lee–Yang–Parr) hybrid functional was employed using the 6-31G* basis set for H, C, N, and O and the SDD (Stuttgart/Dresden) basis for Rh.[39] Following optimization of the molecular structures in C_1 symmetry, frequency analysis was performed to ensure the existence of local minima on the potential energy surfaces. Electronic absorption transitions were calculated using time-dependent DFT (TD-DFT) calculations with polarizable continuum models (PCM) that mimicked the solvation effects of H_2O and CH_3CN.[40] A Gaussian single point calculation was performed on each optimized structure, and GaussSum 1.0 was used to quantify the localization of electron density.[41]

RESULTS AND DISCUSSION

Synthesis and Characterization. The alkylating agent trimethyloxonium (Me_3OBF_4) methylates two acetato ligands of $Rh_2(O_2CCH_3)_4$ (**1**) at room temperature, resulting in the dissociation of two methyl esters and in the generation of *cis*-$[Rh_2(O_2CCH_3)_2(CH_3CN)_6]^{2+}$ (**3**).[28] At elevated temperatures and extended reaction times, all four acetato ligands are methylated by Me_3OBF_4, producing $[Rh_2(CH_3CN)_{10}]^{4+}$.[42] Although a number of dirodium paddlewheel complexes, including $Rh(HNOCCH_3)_4$[27] and $Rh_2[(PhN)_2CH]_4$,[43] have been reported, to our knowledge no studies of their reactivity with alkylating agents have been published.

The reaction of $Rh(HNOCCH_3)_4$ (**2**) with Me_3OBF_4 in CH_3CN produced a mixture of the head-to-tail, (*H,T*) and head-to-head (*H,H*) isomers of *cis*-$[Rh_2(HNOCCH_3)_2(CH_3CN)_6]^{2+}$, complexes **4** and **5**, respectively. The two isomers were separated by fractional precipitation using CH_3CN/CH_2Cl_2 (1:1, v:v) because **4** is highly soluble, whereas **5** is insoluble, in this solvent mixture. Two peaks were observed for **4** and **5** using electrospray ionization mass spectrometry at mass-to-charge (m/z) ratios of 201.98 and 243.01, corresponding to $[Rh_2(HNOCCH_3)_2(CH_3CN)_2]^{2+}$ and $[Rh_2(HNOCCH_3)_2(CH_3CN)_4]^{2+}$, respectively. In addition, the percentages of carbon, nitrogen, and oxygen determined by elemental analysis are consistent with a molecular formula of $[Rh_2(HNOCCH_3)_2(CH_3CN)_4(H_2O)_2][BF_4]_2$ for each isomer.

The molecular structures of **4** and **5** (Figure 2) were determined by single crystal X-ray diffraction (crystallographic details in Table S1), and more detailed information is provided in the Supporting Information (Tables S2 and S3). The Rh–Rh bonds of **4** and **5** are 2.5552(7) and 2.5608(5) Å, respectively (Table 1), which are similar to that of **3**, 2.534(1) Å, but are relatively long for dirhodium paddlewheel complexes with four bridging ligands with Rh–Rh distances in the 2.35–2.45 Å range.[44] Complexes **4** and **5** each have three types of CH_3CN ligands: two equatorial CH_3CN ligands *trans* to the amidato O atoms, $CH_3CN_{eq}^{O}$, two equatorial CH_3CN ligands *trans* to the amidato N atoms, $CH_3CN_{eq}^{N}$, and two axial CH_3CN ligands positioned along the internuclear Rh–Rh axis, CH_3CN_{ax}. The Rh–$CH_3CN_{eq}^{O}$ bonds of **4** and **5** are slightly shorter the Rh–$CH_3CN_{eq}^{N}$ bonds by ~0.03 Å, and similar in length to the Rh-$CH_3CN_{eq}^{O}$ bonds of **3** (Table 1). The Rh–CH_3CN_{ax} bonds of **4** and **5** are significantly longer (by ~0.23 Å) than the Rh–CH_3CN_{eq} bonds, a difference that is also observed in **3** and in $[Rh_2(CH_3CN)_{10}]^{4+}$.[42] Dirhodium complexes generally exhibit

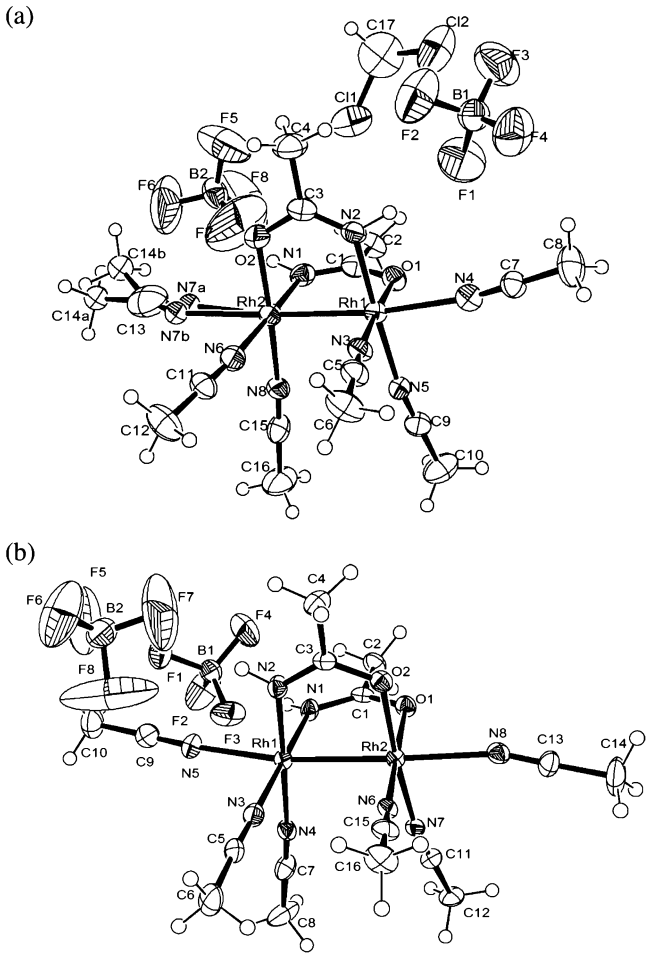

Figure 2. ORTEP plots for (a) **4** and (b) **5** (all ellipsoids drawn at 50% probability; H atoms drawn with artificial radii).

Table 1. Rh–Rh Bond Lengths (Å) and Selected Average Bond Lengths (Å) for 3–5

complex	Rh–Rh	Rh–O_{bridge}	Rh–N_{bridge}	Rh–L_{eq}^{O}	Rh–L_{eq}^{N}	Rh–L_{ax}
3[a]	2.534(1)	2.015		1.983		2.232
4	2.5552(7)	2.023	1.996	1.988	2.035	2.235
5	2.5608(5)	2.016	1.995	2.004	2.026	2.242

[a]From ref 28.

long, weak Rh–CH_3CN_{ax} bonds, and axial ligands are readily displaced by coordinating solvent molecules. This lability explains the positional variability of one CH_3CN_{ax} ligand in the crystal structure of **4** apparent in Figure 2, discussed in the Experimental Section in more detail.

The ^1H NMR spectra of **4** and **5** are shown in Figures S1b and S1c, respectively, and are compared to that of **3** in Figure S1a. The ^1H NMR spectrum of **5** in D_2O (Figure S1c) exhibits three singlets of equal intensity at 2.07, 2.53, and 2.61 ppm, assigned to the two amidato $-CH_3$ groups, the $CH_3CN_{eq}^{N}$ ligands, and the $CH_3CN_{eq}^{O}$ ligands, respectively, on the basis of comparisons among **1**–**3**. No resonances are observed for the CH_3CN_{ax} ligands, but instead a peak at 2.10 ppm is observed (Figure S1c), which corresponds to free CH_3CN resulting from the axial ligands displaced by solvent D_2O molecules (Figure S1c). The ^1H NMR spectrum of **4** in D_2O is similar to that of **5**, with singlets at 2.08, 2.56, and 2.58 ppm assigned to the

dx.doi.org/10.1021/ic3017886 | Inorg. Chem. 2012, 51, 11882–11890

protons of the amidato methyl groups, the $CH_3CN_{eq}{}^N$ ligands, and the $CH_3CN_{eq}{}^O$ ligands, respectively (Figure S1b).

Electronic Absorption, Electronic Structure Calculations, and Electrochemistry. The absorption spectrum of **4** in CH_3CN shown in Figure S2a exhibits maxima at 345 nm (ε = 650 M^{-1} cm^{-1}) and 500 nm (ε = 228 M^{-1} cm^{-1}). Similarly, a shoulder at 350 nm (ε = 410 M^{-1} cm^{-1}) and a peak at 495 nm (ε = 176 M^{-1} cm^{-1}) are observed for **5** in CH_3CN (Figure S2a). These bands are blue-shifted relative to the absorption maxima of **3** at 363 nm (ε = 520 M^{-1} cm^{-1}) and 525 nm (ε = 218 M^{-1} cm^{-1}) in CH_3CN (Figure S2a). The higher energy band of **3** has been assigned to a combination of transitions from metal-based $Rh_2(\pi^*)$ molecular orbitals (MOs) to $Rh-CH_3CN_{eq}(\sigma^*)$ and $Rh_2(\sigma^*)$ MOs, and that at lower energy to a metal-centered $Rh_2(\pi^*)\rightarrow Rh_2(\sigma^*)$ transition.[22] In H_2O, the CH_3CN_{ax} ligands of **3**–**5** are replaced by H_2O molecules, and the absorption maxima for all three complexes shift to longer wavelengths (Figure S2b), each exhibiting a lowest energy absorption band at ~550 nm (Table 2).

Table 2. Experimental and Calculated Absorption Maxima of 3–5 in H_2O, Electrochemical Reduction Potentials, and Quantum Yields for Photoaquation with 400 and 550 nm Irradiation

complex	λ_{exp}/nm (ε/M^{-1} cm^{-1})	λ_{calc}/nm (f)	$E_{1/2}$/V[a]	Φ_{400nm}[b]	Φ_{550nm}[b]
3	555 (160)[c]	551 (0.0005)	−0.56,[d] −0.99[d]	0.13	0.07
4	550 (110)	556 (0.0003)	+1.63, −0.81[d]	0.43	0.14
5	550 (90)	558 (0.0006)	+1.65, −0.84[d]	0.38	0.12

[a]Versus SCE in CH_3CN with 0.1 M Bu_4NPF_6. [b]In H_2O, for the formation of $[Rh_2(LL)_2(CH_3CN)_3(H_2O)_3]^{2+}$ (LL = CH_3COO^-, $HNCCH_3O^-$). [c]From ref 22. [d]Irreversible.

To aid in the assignment of the absorption bands, the model complexes *cis*-$[Rh_2(O_2CH)_2(CH_3CN)_4(H_2O_{ax})_2]^{2+}$ (**3a**), *cis-H,T*-$[Rh_2(HNOCH)_2(CH_3CN)_4(H_2O_{ax})_2]^{2+}$ (**4a**), and *cis-H,H*-$[Rh_2(HNOCH)_2(CH_3CN)_4(H_2O_{ax})_2]^{2+}$ (**5a**) were used to perform electronic structure calculations. The LUMOs for **3a**–**5a** were calculated to be $Rh_2(\sigma^*)$ in character in each complex (Figure S3), consistent with that of **1**, which has been extensively investigated.[45] The HOMOs of **4a** and **5a** are Rh_2–acam(π^*) in character with contributions from the $Rh_2(\delta^*)$ and ligand-centered acam(π^*) orbitals, such that the resulting MO possesses significant electron density on the amidato ligands. In contrast, the HOMO of **3a** is nearly purely metal-centered $Rh_2(\pi^*)$ in character (Figure 3). The LUMO + 1 orbitals of **3a**–**5a** were calculated to be $Rh-CH_3CN_{eq}(\sigma^*)$, with antibonding electron density localized directly on the CH_3CN_{eq} ligands (Figure 3). It should be noted that, in complexes **4a** and **5a**, the $Rh-CH_3CN(\sigma^*)$ character in the LUMO + 1 is concentrated on the CH_3CN ligands positioned *trans* to the oxygen atoms of the bridging acam ligand (Figure 3b,c). Calculations were also performed on the parent paddlewheel model complexes $Rh_2(O_2CH)_4(H_2O_{ax})_2$ (**1a**) and $Rh_2(HNOCH)_4(H_2O_{ax})_2$ (**2a**), and the molecular orbital diagrams for **1a**–**5a** are shown in Figure 4. The HOMOs of **4a** and **5a** are predicted to be isoenergetic and to lie 0.952 eV above that of **3a** and 1.823 eV below that of **2a**. The LUMOs of **4a** and **5a** are also calculated at the same energy, and are

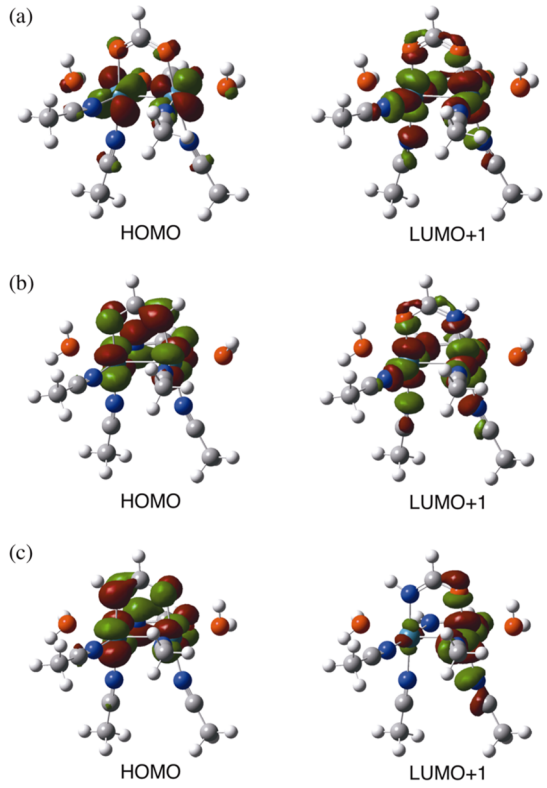

Figure 3. Electron densities of the HOMO and the LUMO + 1 molecular orbitals of (a) **3**, (b) **4**, and (c) **5** plotted with isovalue = 0.4.

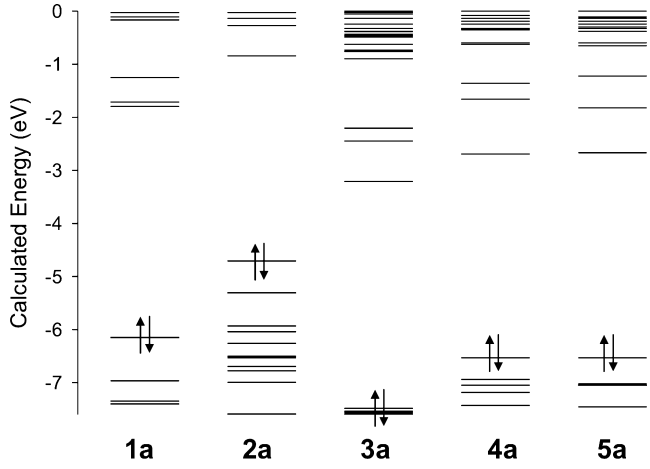

Figure 4. Calculated molecular orbitals diagrams for **1a**–**5a**.

positioned 0.531 eV higher in energy than that of **3a**, but 1.837 eV lower in energy than that of **2a** (Figure 4).

The reduction and oxidation potentials for **3**–**5** were determined by cyclic voltammetry and are listed in Table 2. The stepwise oxidation of **2** was previously reported with $E_{1/2}(Rh_2^{III,II/II,II})$ = +0.15 V versus SCE and $E_{1/2}(Rh_2^{III,III/III,II})$ = +1.41 V versus SCE in CH_3CN, whereas only the first oxidation process is observed for **1** at $E_{1/2}(Rh_2^{III,II/II,II})$ = +1.17 V versus SCE in the same solvent.[46] The $Rh_2^{III,II/II,II}$ couple was not observed for **3** up to +2.00 V versus SCE in CH_3CN, but is present in **4** and **5** at +1.63 and +1.65 V versus SCE, respectively (Table 2). No reduction peaks were observed for **1** and **2** up to −1.50 V versus SCE, but two irreversible waves were observed for **3** at −0.56 and −0.99 V versus SCE, and **4**

dx.doi.org/10.1021/ic3017886 | *Inorg. Chem.* 2012, 51, 11882–11890

and **5** each exhibited one irreversible wave at −0.81 and −0.84 V versus SCE, respectively (Table 2).

The experimental electrochemistry data is consistent with the trends predicted by the DFT calculations, specifically that the redox potentials of **4** and **5** are similar, that **3** is the most difficult complex of the series to oxidize, and that **4** and **5** are more difficult to reduce than **3** (Figure 4). On the basis of the experimental redox potentials of **4** and **5** and the calculated relative energies of the HOMOs of **3a**−**5a**, it is predicted that the oxidation of **3** should occur at approximately +2.6 V. Similarly, the first reduction of **1** and **2** can be predicted at approximately −1.8 and −2.6 V, respectively, when compared to the experimental values for **4** and **5** and the relative energies of the LUMOs calculated for **1a**−**5a**. To our knowledge, no reduction potentials have been reported for **1** and **2**, and no electrochemistry data has been published for **3**.

The low-energy electronic transitions for **3a**−**5a** were predicted using time-dependent DFT (TD-DFT) methods, and the calculated lowest energy absorption maxima (λ_{calc}) in H_2O (Table 2) and CH_3CN agree well with the experimental absorption maxima (λ_{exp}) in each solvent (Table S4). In H_2O, excitation of **3a** at 551 nm is predicted to depopulate the $Rh_2(\pi^*)$ HOMO and HOMO − 2 orbitals and populate the $Rh_2(\sigma^*)$ LUMO and Rh−$CH_3CN_{eq}(\sigma^*)$ LUMO + 1 orbitals (Figure 3a and Table S4), consistent with calculations previously reported for **3a** in the gas phase.[22] The lowest energy excited state of **4a** in H_2O is calculated at 556 nm and corresponds to the depopulation of the HOMO and HOMO − 2 orbitals and population of the LUMO. In contrast to **3a**, the HOMO of **4a** has significant ligand character, with 15% of the total electron density residing on the amidato ligands, in the Rh_2−acam(π^*) orbital (Figure 3). Therefore, excitation of **4a** at 556 nm is predicted to induce Rh_2−acam(π^*) → $Rh_2(\sigma^*)$ transitions. Similarly, excitation of **5a** at 558 nm in H_2O is expected to depopulate the HOMO − 3, HOMO − 2, HOMO − 1, and HOMO levels and to populate the LUMO. The HOMO of **5a** is similar to that of **4a**, such that Rh_2-acam(π^*) → $Rh_2(\sigma^*)$ transitions are also predicted.

Photochemistry in Solution. Photochemical experiments show that **4** and **5** exhibit similar reactivity as **3**, which has been shown to exchange two CH_3CN_{eq} ligands for water molecules upon irradiation with visible light.[22] The photolysis of **4** with visible light ($\lambda_{irr} \geq 495$ nm) in D_2O results in the disappearance of the ^1H NMR peaks associated with the reactant, R, at 2.58, 2.56, and 2.08 ppm and the appearance of free CH_3CN, F, at 2.10 ppm and product peaks, labeled *, in the 1.94−2.64 ppm range (Figure 5). After 60 min of irradiation, the reactant peaks are nearly depleted, the peaks associated with photoproducts are prominent, and on the basis of the integration of the free CH_3CN peak, 2 equiv of free CH_3CN are present (Figure 5). Similarly, the photolysis of **5** in D_2O ($\lambda_{irr} \geq 495$ nm) also results in the depletion of the starting material, an increase in free CH_3CN, which integrates to 2 equiv after 60 min of irradiation, and the appearance of product peaks between 2.00 and 2.68 ppm (Figure S4).

The irradiation of **4** and **5** with visible light results in the exchange of two CH_3CN_{eq} ligands for D_2O molecules, but it is unclear from the experiments in D_2O if one type of equatorial ligand, $CH_3CN_{eq}{}^{O}$ and $CH_3CN_{eq}{}^{N}$, exchanges preferentially with respect to the other. To answer this question, the photolysis of **4** and **5** was performed in CD_3CN, in which the CD_3CN-substituted photoproducts are isoelectronic with the starting material. The irradiation of **4** in CD_3CN ($\lambda_{irr} \geq 495$ nm) shows that both the $CH_3CN_{eq}{}^{O}$ and the $CH_3CN_{eq}{}^{N}$ ligands, at 2.44 and 2.43 ppm, respectively, exchange with CD_3CN molecules, as indicated by the decrease in intensity of the two bands relative to an internal benzene standard (Figure S5). Similarly, the photolysis of **5** in CD_3CN ($\lambda_{irr} \geq 495$ nm) revealed that both the $CH_3CN_{eq}{}^{O}$ ligands, at 2.48 ppm, and the $CH_3CN_{eq}{}^{N}$ ligands, at 2.40 ppm, exchange with CD_3CN solvent molecules when the complex is irradiated (Figure S6). The data indicate that the exchange of the $CH_3CN_{eq}{}^{O}$ ligands is slightly more facile than that of the $CH_3CN_{eq}{}^{N}$ ligands upon irradiation.

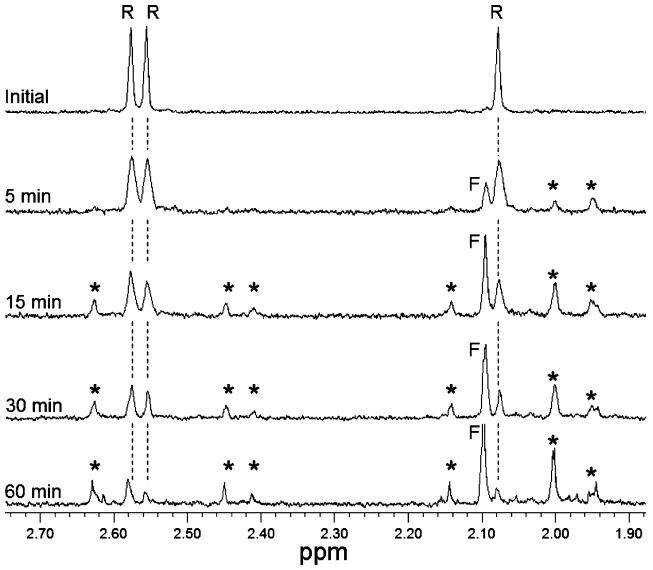

Figure 5. Changes to the ^1H NMR spectrum of **4** in D_2O as a function of irradiation time ($\lambda_{irr} \geq 495$ nm), where the labels R, F, and * represent peaks associated with the starting material free CH_3CN, and product, respectively.

The photochemistry of **4** and **5** was further investigated using electronic absorption spectroscopy, and was compared to that of **3** under similar experimental conditions. The irradiation of **3** in H_2O with near-UV light results in a shift of the reactant peak at 555−573 nm ($\lambda_{irr} \geq 345$ nm, 10.5 h),[22] whereas irradiation with lower energy light ($\lambda_{irr} \geq 495$ nm, 0−60 min) results in only slight reactivity with negligible spectra changes (Figure 6a). In contrast, the decrease in intensity of the 363 and 550 nm absorption features of **4** are evident in Figure 6b, with the concomitant increase of a broad peak with maximum at 581 nm ($\lambda_{irr} \geq 495$ nm, 0−60 min). Similarly, the absorption bands of **5** at 371 and 550 nm in H_2O decrease in intensity, and a new band at 575 nm appears as a function of irradiation time (Figure 6c). The quantum yields measured for **3** in H_2O with 400 and 500 nm irradiation are listed in Table 2 and are consistent with those previously reported, $\Phi_{355} = 0.37$ and $\Phi_{509} = 0.09$.[22] Complexes **4** and **5** exhibit ∼3-fold (400 nm) and ∼2-fold (500 nm) greater quantum yields in H_2O than those of **3** (Table 2), a desirable property for potential photochemotherapy applications. It is important to note that no spectral changes are observed for **4** and **5** in D_2O (^1H NMR, Figures S7 and S8) or in H_2O (electronic absorption, Figure S9) when the complexes are kept in the dark at room temperature for 0−60 min.

The MOs involved in the lowest energy transitions of **4** and **5** were evaluated to help explain the enhanced photoinduced ligand exchange yields of these complexes as compared to that of **3** with $\lambda_{irr} \geq 495$ nm. Excitation of **4** and **5** with 556 and 558

dx.doi.org/10.1021/ic3017886 | Inorg. Chem. 2012, 51, 11882−11890

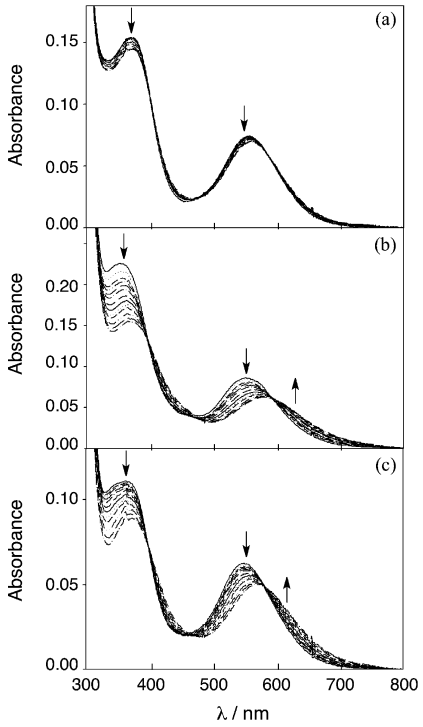

Figure 6. Changes to the electronic absorption spectra of (a) **3**, (b) **4**, and (c) **5** in H_2O as a function of irradiation time ($\lambda_{irr} \geq 495$ nm, 0–60 min).

nm light, respectively, is predicted to depopulate the Rh_2–acam(π^*) HOMOs of these complexes (Figure 3). It is proposed that depopulation of this orbital strengthens the Rh–acam bond and weakens the Rh–CH_3CN_{eq} bonds positioned *trans* to the acetamide ligands, thus enhancing the dissociation of the CH_3CN_{eq} ligands. This mechanism requires a ligand-based HOMO to be operative and is not predicted to occur in **3**, which has a metal-centered $Rh_2(\pi^*)$ HOMO. Instead, the photoinduced ligand exchange for **3** is believed to result from population of the Rh–$CH_3CN_{eq}(\sigma^*)$ LUMO + 1 orbital, as previously reported.[22] The greater ligand exchange quantum yields observed for **4** and **5** as compared to **3** may therefore be ascribed to the presence and depopulation of the ligand-based Rh_2-acam(π^*) HOMO in the former.

Photoinduced DNA Binding. The photoproducts of **3** and the thermally activated form of cisplatin bind to linearized ds-DNA to yield adducts that have reduced electrophoretic mobility in agarose gels.[5g,22] Gel electrophoresis experiments were performed with **4**, which exhibited the greatest quantum yield of ligand exchange among **3**–**5**. In the two gels shown in Figure 7, lanes 1 and 8 contain a 1 kb DNA ladder, and lanes 2 and 7 were loaded with 50 μM linearized DNA alone. Lanes 3–6 contain 50 μM linearized DNA with increasing concentrations of **4**, where [DNA bases]/[**4**] = 0.33, 0.17, 0.11, and 0.08, respectively. In Figure 7a, the solutions loaded into lanes 3–6 were irradiated for 15 min ($\lambda_{irr} \geq 495$ nm) prior to electrophoresis, where a progressive decrease in DNA mobility is evident as a function of increasing concentration of **4**. In contrast, no mobility decrease is observed for the same lanes for the control gel, where the DNA and complex were incubated in the dark for 15 min at room temperature (Figure 7b). These data show that the photoproducts of **4** covalently bind to double-stranded DNA following the exchange of the CH_3CN_{eq} ligands with H_2O afforded by irradiation with visible light. It is also evident from the data in Figure 7b that this binding does not take place with the initial unsubstituted complex **4**. Additional DNA mobility studies show that when a higher concentration of **4** is used, lower energy irradiation, approaching the PDT window, can be used to activate **4**. The gel shows that low energy irradiation ($\lambda_{irr} \geq 610$ nm, 30 min) generates photoproducts of **4** that bind to DNA, and no binding is evident in the dark (Figure 7c). Additional experiments show that there is no change in the absorption spectra of **4** and **5** in the presence of calf-thymus DNA in the dark for 60 min (Figures S10 and S11), also consistent with the absence of binding by the parent complexes. It is evident from Figures S10 and S11 that irradiation of **4** and **5** in buffer ($\lambda_{irr} \geq 395$ nm), followed by the addition of DNA, results in absorption changes consistent with the interaction of the photoproduct with the duplex.

■ CONCLUSIONS

The head-to-tail, *H,T*, and head-to-head, *H,H*, isomers of *cis*-$[Rh_2(HNOCCH_3)_2(CH_3CN)_6]^{2+}$ were synthesized and characterized for the first time, **4** and **5**, respectively. Each complex contains two axial CH_3CN ligands that exchange rapidly with coordinating solvent molecules, as well as two types of

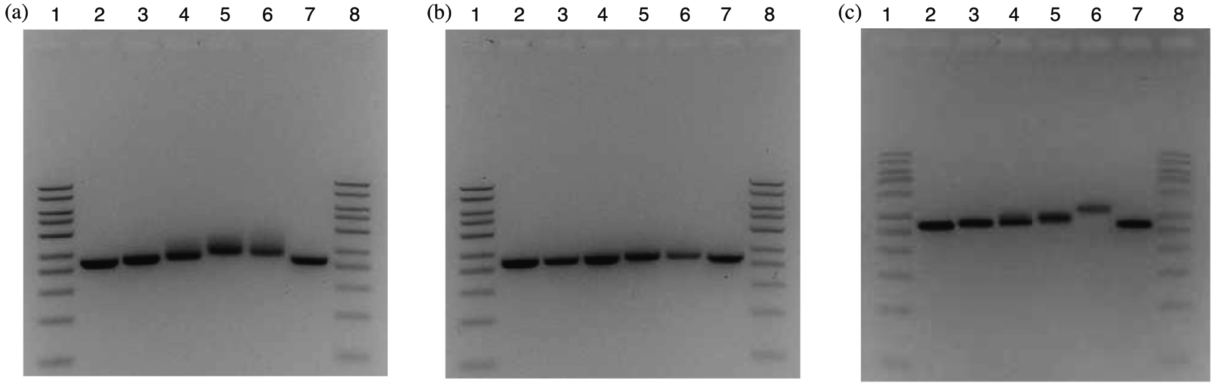

Figure 7. Imaged ethidium bromide-stained agarose gels with 50 μM linearized pUC19 plasmid (10 mM phosphate, pH = 7.5) in the presence of **4**. (a–c) Lanes 1 and 8, 1 kb DNA molecular weight standard; lanes 2 and 7, DNA only. (a) Irradiated ($\lambda_{irr} \geq 495$ nm, 15 min) and (b) incubated in the dark at 25 °C for 15 min; lanes 3–6 [DNA bases]/[**4**] = 0.33, 0.17, 0.11, 0.08. (c) [DNA]/[**4**] = 0.01 (30 min incubation or irradiation) in lanes 3–6; lane 3, dark; lane 4, $\lambda_{irr} \geq 695$; lane 5, $\lambda_{irr} \geq 645$ nm; lane 6, $\lambda_{irr} \geq 610$ nm.

dx.doi.org/10.1021/ic3017886 | *Inorg. Chem.* 2012, 51, 11882–11890

equatorial CH_3CN ligands, $CH_3CN_{eq}^{O}$ and $CH_3CN_{eq}^{N}$, which do not exchange with solvent molecules at room temperature when kept in the dark. The photolysis of **4** and **5** in water promotes the exchange of two CH_3CN_{eq} ligands for H_2O molecules, and both the $CH_3CN_{eq}^{O}$ and $CH_3CN_{eq}^{N}$ ligands exchange in equal proportions, as determined by ^1H NMR spectroscopy. The ligand exchange quantum yields for **4** and **5** were measured with to be ~3-fold (λ_{irr} = 400 nm) and ~2-fold (λ_{irr} = 500 nm) greater than those previously reported for the related complex *cis*-$[Rh_2(O_2CCH_3)_2(CH_3CN)_6]^{2+}$ (**3**). Electronic structure calculations show that the HOMOs of **4** and **5** have significant bridging ligand contribution with Rh_2−acam(π^*) character, whereas that of **3** is $Rh_2(\pi^*)$, localized on the metal. This difference may explain enhanced quantum yields for **4** and **5** as compared to that of **3**, where the depopulation of the Rh_2−acam(π^*) antibonding HOMOs in the former is expected to strengthen the Rh_2−acam bonds, while simultaneously weakening those to the equatorial CH_3CN ligands, Rh−CH_3CN_{eq}, that are positioned *trans* to the bridging acam ligands. DNA mobility shift assays show that **4**, while inactive in the dark, binds to linearized DNA upon irradiation with low energy light (λ_{irr} > 610 nm). This result shows that **4** may be considered a potential agent for photochemotherapy that is independent of the presence of oxygen.

■ ASSOCIATED CONTENT

Ⓢ Supporting Information

NMR spectra of **3**−**5**, crystallographic information, calculations, electronic absorption spectra of **3**−**5**, additional data from calculations, additional photochemistry data and controls. This material is available free of charge via the Internet at http://pubs.acs.org.

■ AUTHOR INFORMATION

Corresponding Author

*E-mail: turro.1@osu.edu.

Notes

The authors declare no competing financial interest.

■ ACKNOWLEDGMENTS

We thank the National Science Foundation for partial support of this work (CHE-1213646) and the Ohio Supercomputer Center for valuable resources.

■ REFERENCES

(1) (a) Rosenberg, B.; Van Camp, L.; Krigas, T. *Nature* **1965**, *205*, 698−699. (b) Rosenberg, B.; Van Camp, L.; Trosko, J. E.; Mansour, V. H. *Nature* **1969**, *222*, 385−386.

(2) (a) Dhar, S.; Lippard, S. J. Current Status and Mechanism of Action of Platinum-Based Anticancer Drugs. In *Bioinorganic Medicinal Chemistry*; Alessio, E., Ed.; Wiley-VCH: Weinheim, 2011; pp 79−86. (b) Ang, W. H.; Myint, M. N. Z.; Lippard, S. J. *J. Am. Chem. Soc.* **2010**, *132*, 7429−7435. (c) Todd, R. C.; Lippard, S. J. *J. Inorg. Biochem.* **2010**, *104*, 902−908. (d) Kelland, L. *Nat. Rev. Cancer* **2007**, *7*, 573−584. (e) Jung, Y.; Lippard, S. J. *Chem. Rev.* **2007**, *107*, 1387−1407. (f) Mantri, Y.; Lippard, S. J.; Baik, M. H. *J. Am. Chem. Soc.* **2007**, *129*, 5023−5030. (g) Wang, D.; Lippard, S. J. *Nat. Rev. Drug Discov.* **2005**, *4*, 307−320. (h) Jamieson, E. R.; Lippard, S. J. *Chem. Rev.* **1999**, *99*, 2467−2498. (i) Go, R. S.; Adjei, A. A. *J. Clin. Oncol.* **1999**, *17*, 409−422. (j) Zamble, D. B.; Lippard, S. J. *Trends Biochem. Sci.* **1995**, *20*, 435−439. (k) *Platinum-Based Drugs in Cancer Therapy*; Kelland, L. R., Farell, N., Eds.; Humana: Totowa, NJ, 2000. (l) *Cisplatin: Chemistry and Biochemistry of a Leading Anticancer Drug*; Lippert, B., Ed.; Wiley-VCH: Wurzburg, Germany, 1999. (m) Rajski, S. R.; Williams, R. M. *Chem. Rev.* **1998**, *98*, 2723−2795.

(3) (a) Wheate, N. J.; Walker, S.; Craig, G. E.; Oun, R. *Dalton Trans.* **2010**, *39*, 8097−8340. (b) Olszewski, U.; Hamilton, G. *Anticancer Agents Med. Chem.* **2010**, *10*, 293−301. (c) Galanski, M.; Jakupec, M. A.; Keppler, B. K. *Curr. Med. Chem.* **2005**, *12*, 2075−2094.

(4) (a) Wilson, J. J.; Lippard, S. J. *Inorg. Chem.* **2011**, *50*, 3103−3115. (b) Hochreuther, S.; Puchta, R.; van Eldik, R. *Inorg. Chem.* **2011**, *50*, 8984−8996. (c) Varbanov, H.; Valiahdi, S. M.; Legin, A. A.; Jakupec, M. A.; Roller, A.; Galanski, M.; Keppler, B. K. *Eur. J. Med. Chem.* **2011**, *46*, 5456−5464. (d) Reithofer, M. R.; Bytzek, A. K.; Valiahdi, S. M.; Kowol, C. R.; Groessl, M.; Hartinger, C. G.; Jakupec, M. A.; Galanski, M.; Keppler, B. K. *J. Inorg. Biochem.* **2011**, *105*, 46−51. (e) Štarha, P.; Trávníček, Z.; Popa, I. *J. Inorg. Biochem.* **2010**, *104*, 639−647. (f) Wagner, G.; Marchant, A.; Sayer, J. *Dalton Trans.* **2010**, *39*, 7747−7759. (g) Scaffidi-Domianello, Y. Y.; Meelich, K.; Jakupec, M. A.; Arion, V. B.; Kukushkin, V. Y.; Galanski, M.; Keppler, B. K. *Inorg. Chem.* **2010**, *49*, 5669−5678. (h) Mangrum, J. B.; Farrell, N. P. *Chem. Commun.* **2010**, *46*, 6640−6650. (i) Gwak, H.-S.; Shingu, T.; Chumbalkar, V.; Hwang, Y.-H.; DeJournett, R.; Latha, K.; Koul, D.; Yung, W. K.; Powis, G.; Farrell, N. P.; Bögler, O. *Int. J. Cancer* **2010**, *128*, 787−796. (j) Marverti, G.; Cusumano, M.; Ligabue, A.; Di Pietro, M. L.; Vainiglia, P. A.; Ferrari, A.; Bergomi, M.; Moruzzi, M. S.; Frassineti, C. *J. Inorg. Biochem.* **2008**, *102*, 699−712.

(5) (a) Kang, M.; Chifotides, H. T.; Dunbar, K. R. *Biochemistry* **2008**, *47*, 2265−2276. (b) Chifotides, H. T.; Dunbar, K. R. *Chem.—Eur. J.* **2008**, *14*, 9902−9913. (c) Chifotides, H. T.; Dunbar, K. R. *J. Am. Chem. Soc.* **2007**, *129*, 12480−12490. (d) Deubel, D. V.; Chifotides, H. T. *Chem. Commun.* **2007**, 3438−3440. (e) Aguirre, J. D.; Lutterman, D. A.; Angeles-Boza, A. M.; Dunbar, K. R.; Turro, C. *Inorg. Chem.* **2007**, *46*, 7494−7502. (f) Chifotides, H. T.; Dunbar, K. R. *Chem.—Eur. J.* **2006**, *12*, 6458−6468. (g) Dunham, S. U.; Chifotides, H. T.; Mikulski, S.; Burr, A. E.; Dunbar, K. R. *Biochemistry* **2005**, *44*, 996−1003. (h) Chifotides, H. T.; Fu, P. K.-L.; Dunbar, K. R.; Turro, C. *Inorg. Chem.* **2004**, *43*, 1175−1183. (i) Chifotides, H. T.; Koomen, J. M.; Kang, M.; Tichy, S. E.; Dunbar, K. R.; Russell, D. H. *Inorg. Chem.* **2004**, *43*, 6177−6187. (j) Chifotides, H. T.; Koshlap, K. M.; Pérez, L. M.; Dunbar, K. R. *J. Am. Chem. Soc.* **2003**, *125*, 10703−10713. (k) Chifotides, H. T.; Koshlap, K. M.; Pérez, L. M.; Dunbar, K. R. *J. Am. Chem. Soc.* **2003**, *125*, 10714−10724. (l) Aoki, K.; Salam, M. A. *Inorg. Chim. Acta* **2002**, *339*, 427−437. (m) Catalan, K. V.; Mindiola, D. J.; Ward, D. L.; Dunbar, K. R. *Inorg. Chem.* **1997**, *36*, 2458−2460.

(6) (a) Howard, R. A.; Kimball, A. P.; Bear, J. L. *Cancer Res.* **1979**, *39*, 2568−2573. (b) Erck, A.; Rainen, L.; Whileyman, J.; Chang, I. M.; Kimball, A. P.; Bear, J. *Proc. Soc. Exp. Biol. Med.* **1974**, *145*, 1278−1283.

(7) (a) Aguirre, J. D.; Angeles-Boza, A. M.; Chouai, A.; Pellois, J.-P.; Turro, C.; Dunbar, K. R. *J. Am. Chem. Soc.* **2009**, *131*, 11353−11360. (b) Aguirre, J. D.; Angeles-Boza, A. M.; Chouai, A.; Turro, C.; Pellois, J.-P.; Dunbar, K. R. *Dalton Trans.* **2009**, *48*, 10806−10812. (c) Angeles-Boza, A. M.; Chifotides, H. T.; Aguirre, J. D.; Chouai, A.; Fu, P. K.; Dunbar, K. R.; Turro, C. *J. Med. Chem.* **2006**, *49*, 6841−6847. (d) Clarke, M. J.; Zhu, F.; Frasca, D. R. *Chem. Rev.* **1999**, *99*, 2511−2533.

(8) Szacilowski, K.; Macyk, W.; Drzewiecka-Matuszek, A.; Brindell, M.; Stochel, G. *Chem. Rev.* **2005**, *105*, 2647−2694.

(9) (a) Celli, J. P.; Spring, B. Q.; Rizvi, I.; Evans, C. L.; Samkoe, K. S.; Verma, S.; Pogue, B. W.; Hasan, T. *Chem. Rev.* **2010**, *110*, 2795−2838. (b) Allison, R. R.; Sibata, C. H. *Photodiagn. Photodyn. Ther* **2010**, *7*, 61−75. (c) Wolkenberg, S. E.; Boger, D. L. *Chem. Rev.* **2002**, *102*, 2477−2496. (d) Dougherty, T. J.; Gomer, C. J.; Henderson, B. W.; Jori, G.; Kessel, D.; Korbelik, M.; Moan, J.; Peng, Q. *J. Natl. Cancer Inst.* **1998**, *90*, 889−905.

(10) (a) Svanberg, K.; Bendsoe, N.; Axelsson, J.; Andersson-Engels, S.; Svanberg, S. *J. Biomed. Opt.* **2010**, *15*, 041502. (b) Nyst, H. J.; Tan, I. B.; Stewart, F. A.; Balm, A. J. M. *Photodiagn. Photodyn. Ther.* **2009**, *6*, 3−11. (c) O'Connor, A. E.; Gallagher, W. M.; Byrne, A. T. *Photochem. Photobiol.* **2009**, *85*, 1053−1074. (d) Juarranz, A.; Jaén, P.; Sanz-Rodríguez, F.; Cuevas, J.; González, S. *Clin. Transl. Oncol.* **2008**, *10*,

148−154. (e) Moghissi, K.; Dixon, K. *Photodiagn. Photodyn. Ther.* **2008**, *5*, 10−18. (f) Zuluaga, M.-F.; Lange, N. *Curr. Med. Chem.* **2008**, *15*, 1655−1673. (g) Gray, J.; Fullarton, G. *Photodiagn. Photodyn. Ther.* **2007**, *4*, 151−159.
(11) Lovell, J. F.; Liu, T. W. B.; Chen, J.; Zheng, G. *Chem. Rev.* **2010**, *110*, 2839−2857.
(12) (a) DeRosa, M. C.; Crutchley, R. J. *Coord. Chem. Rev.* **2002**, *233*−*234*, 351−371. (b) Allen, C. M.; Sharman, W. M.; van Lier, J. E. *Tumor Targeting Cancer Ther.* **2002**, 329−361. (c) Hsi, R. A.; Rosenthal, D. I.; Glatstein, E. *Drugs* **1999**, *57*, 725−734.
(13) (a) Harris, A. L. *Nat. Rev. Cancer* **2002**, *2*, 38−47. (b) Shannon, A. M.; Bouchier-Hayes, D. J.; Condron, C. M.; Toomey, D. *Cancer Treat. Rev.* **2003**, *29*, 297−307.
(14) Ali, H.; van Lier, E. *Chem. Rev.* **1999**, *99*, 2379−2450.
(15) (a) Joyce, L. E.; Aguirre, J. D.; Angeles-Boza, A. M.; Chouai, A.; Fu, P. K.-L.; Dunbar, K. R.; Turro, C. *Inorg. Chem.* **2010**, *49*, 5371−5376. (b) Sun, Y.; Joyce, L. E.; Dickson, N. M.; Turro, C. *Chem. Commun.* **2010**, *46*, 6759−6761. (c) Sun, Y.; Joyce, L. E.; Dickson, N. M.; Turro, C. *Chem. Commun.* **2010**, *46*, 2426−2428. (d) Zhao, R.; Hammitt, R.; Thummel, R. P.; Liu, Y.; Turro, C. *Dalton Trans.* **2009**, 10926−10931. (e) Liu, Y.; Hammitt, R.; Lutterman, D. A.; Joyce, L. E.; Thummel, R. P.; Turro, C. *Inorg. Chem.* **2009**, *48*, 375−383. (f) Zigler, D. F.; Wang, J.; Brewer, K. J. *Inorg. Chem.* **2008**, *47*, 11342−11350. (g) Angeles-Boza, A. M.; Bradley, P. M.; Fu, P. K.-L.; Shatruk, M.; Hilfiger, M. G.; Dunbar, K. R.; Turro, C. *Inorg. Chem.* **2005**, *44*, 7262−7264.
(16) (a) Delaney, S.; Pascaly, M.; Bhattacharya, P. K.; Hahn, K.; Barton, J. K. *Inorg. Chem.* **2002**, *41*, 1966−1974. (b) Erikklia, K. E.; Odom, D. T.; Barton, J. K. *Chem. Rev.* **1999**, *99*, 2777−2795.
(17) (a) Chouai, A.; Wicke, S. E.; Turro, C.; Bacsa, J.; Dunbar, K. R.; Wang, D.; Thummel, R. P. *Inorg. Chem.* **2005**, *44*, 5996−6003.
(18) (a) Higgins, S. L. H.; White, T. A.; Winkel, B. S. J.; Brewer, K. J. *Inorg. Chem.* **2011**, *50*, 463−470. (b) Prussin, A. J., II; Zhao, S.; Jain, A.; Winkel, B. S. J.; Brewer, K. J. *J. Inorg. Biochem.* **2009**, *103*, 427−431. (c) Jain, A.; Wang, J.; Mashack, E. R.; Winkel, B. S. J.; Brewer, K. J. *Inorg. Chem.* **2009**, *48*, 9077−9084. (d) Williams, R. L.; Toft, N.; Winkel, B.; Brewer, K. J. *Inorg. Chem.* **2003**, *42*, 4394−4400.
(19) (a) Farrer, N. J.; Salassa, L.; Sadler, P. J. *Dalton Trans.* **2009**, *48*, 10690−10701. (b) Salassa, L.; Ruiu, T.; Garino, C.; Pizarro, A. M.; Bardelli, F.; Gianolio, D.; Westendorf, A.; Bednarski, P. J.; Lamberti, C.; Gobetto, R.; Sadler, P. J. *Organometallics* **2010**, *29*, 6703−6710. (c) Farrer, N. J.; Woods, J. A.; Salassa, L.; Zhao, Y.; Robinson, K. S.; Clarkson, G.; Mackay, F. S.; Sadler, P. J. *Angew. Chem., Int. Ed.* **2010**, *49*, 8905−8908. (d) Farrer, N. J.; Woods, J. A.; Munk, V. P.; Mackay, F. S.; Sadler, P. J. *Chem. Res. Toxicol.* **2010**, *23*, 413−421. (e) Ronconi, L.; Sadler, P. J. *Dalton Trans.* **2011**, *40*, 262−268.
(20) (a) Holder, A. A.; Zigler, D. F.; Tarrago-Trani, M. T.; Storrie, B.; Brewer, K. J. *Inorg. Chem.* **2007**, *46*, 4760−4762. (b) Holder, A. A.; Swavey, S.; Brewer, K. J. *Inorg. Chem.* **2004**, *43*, 303−308. (c) Swavey, S.; Brewer, K. J. *Inorg. Chem.* **2002**, *41*, 6196−6198. (d) Armitage, B. *Chem. Rev.* **1998**, *98*, 1171−1200.
(21) Harvey, T. J.; Hennig, I. M.; Shnyder, S. D.; Cooper, P. A.; Ingram, N.; Hall, G. D.; Selby, P. J.; Chester, J. D. *Cancer Gene Ther.* **2011**, *18*, 773−784.
(22) Lutterman, D. A.; Fu, P. K.-L.; Turro, C. *J. Am. Chem. Soc.* **2006**, *128*, 738−739.
(23) (a) Liu, Y.; Turner, D. B.; Singh, T. N.; Angeles-Boza, A. M.; Chouai, A.; Dunbar, K. R.; Turro, C. *J. Am. Chem. Soc.* **2009**, *131*, 26−27. (b) Singh, T.; Turro, C. *Inorg. Chem.* **2004**, *43*, 7260−7262.
(24) (a) Westendorf, A. F.; Zerzankova, L.; Salassa, L.; Sadler, P. J.; Brabec, V.; Bednarski, P. J. *J. Inorg. Biochem.* **2011**, *105*, 652−662. (b) Ronconi, L.; Sadler, P. J. *J. Dalton Trans.* **2011**, *40*, 262−268. (c) Liu, H.-K.; Sadler, P. J. *Acc. Chem. Res.* **2011**, *44*, 348−359. (d) Farrer, N. J.; Woods, J. A.; Salassa, L.; Zhao, Y.; Robinson, K. S.; Clarkson, G.; Mackay, F. S.; Sadler, P. J. *Angew. Chem., Int. Ed.* **2010**, *49*, 8905−8908. (e) Salassa, L.; Ruiu, T.; Garino, C.; Pizarro, A. M.; Bardelli, F.; Gianolio, D.; Westendorf, A.; Bednarski, P. J.; Lamberti, C.; Gobetto, R.; Sadler, P. J. *Organometallics* **2010**, *29*, 6703−6710. (f) Farrer, N. J.; Woods, J. A.; Munk, V. P.; Mackay, F. S.; Sadler, P. J. *Chem. Res. Toxicol.* **2010**, *23*, 413−421. (g) Farrer, N. J.; Salassa, L.; Sadler, P. J. *Dalton Trans.* **2009**, *48*, 10690−10701.
(25) (a) Respondek, T.; Garner, R. N.; Herroon, M. K.; Podgorski, I.; Turro, C.; Kodanko, J. J. *J. Am. Chem. Soc.* **2011**, *133*, 17164−17167. (b) Garner, R. N.; Joyce, L. E.; Turro, C. *Inorg. Chem.* **2011**, *50*, 4384−4391.
(26) Rempel, G. A.; Legzdins, P.; Smith, H.; Wilkinson, G. *Inorg. Syn.* **1971**, *13*, 90−91.
(27) Doyle, M. P.; Bagheri, V.; Wandless, T. J.; Harn, N. K.; Brinker, D. A.; Eagle, C. T.; Loh, K.-L. *J. Am. Chem. Soc.* **1990**, *112*, 1906−1912.
(28) Pimblett, G.; Garner, C. D. *J. Chem. Soc., Dalton Trans.* **1986**, *6*, 1257−1263.
(29) Gottlieb, H. E.; Kotlyar, V.; Nudelman, A. *J. Org. Chem.* **1997**, *62*, 7512−7515.
(30) Gennett, T.; Milner, D. F.; Weaver, M. J. *J. Phys. Chem.* **1985**, *89*, 2787−2794.
(31) Otwinowski, Z.; Minor, W. *Macromolecular Crystallography, Part A*; Methods in Enzymology; Carter, C. W., Jr., Sweet, R. M., Eds.; Academic Press: New York, 1997; Vol. *276*, pp 307−326.
(32) SHELXS-97: Sheldrick, G. M. *Acta Crystallogr.* **2008**, *A64*, 112−122.
(33) SHELXL-97: Sheldrick, G. M., *Acta Crystallogr.* **2008**, *A64*, 112−122.
(34) WinGX-Version 1.70.01: Farrugia, L. J. *J. Appl. Crystallogr.* **1999**, *32*, 837−838.
(35) *International Tables for Crystallography*; Kluwer Academic Publishers: Dordrecht, The Netherlands, 1992; Vol. *C*.
(36) *Handbook of Photochemistry*, 3rd ed.; Montalti, M., Credi, A., Prodi, L., Gandolfi, M. T., Eds.; CRC Press: Boca Raton, FL, 2006; pp 601−616.
(37) Wegner, E. E.; Adamson, A. W. *J. Am. Chem. Soc.* **1966**, *88*, 394−404.
(38) Frisch, M. J.; et al. *Gaussian 03, Revision C.02*; Gaussian, Inc.: Wallingford, CT, 2004.
(39) (a) Becke, A. D. *Phys. Rev.* **1988**, *38*, 3098−3100. (b) Becke, A. D. *J. Chem. Phys.* **1993**, *98*, 1372−1377. (c) Hehre, W. J.; Radom, L.; Schleyer, P. v. R.; Pople, J. A. *Ab Initio Molecular Orbital Theory*; John Wiley and Sons: New York, 1986. (d) Wedig, U.; Dolg, M.; Stoll, H. *Quantum Chemistry: The Challenge of Transition Metals and Coordination Chemistry*; Kluwer Academic Publishers: Boston, 1986. (e) Dolg, M.; Stoll, H.; Preuss, H. *Theor. Chim. Acta.* **1995**, *85*, 441−450.
(40) Fantacci, S.; Angelis, F. D.; Selloni, A. J. *J. Am. Chem. Soc.* **2003**, *125*, 4381−4387.
(41) O'Boyle, N. M.; Tenderholt, A. L.; Langner, K. M. *J. Comput. Chem.* **2008**, *29*, 839−845.
(42) Dunbar, K. R. *J. Am. Chem. Soc.* **1988**, *110*, 8247−8249.
(43) Bear, J. L.; Yao, C.-L.; Lifsey, R. S.; Korp, J. D.; Kadish, K. M. *Inorg. Chem.* **1991**, *30*, 336−340.
(44) Chifotides, H. T.; Dunbar, K. R. Rhodium Compounds. In *Multiple Bonds Between Metal Atoms*, 3rd ed.; Cotton, F. A., Murillo, C., Walton, R. A., Eds., Springer-Science and Business Media, Inc.: New York, 2005; Chapter 12, pp 465−589.
(45) (a) Trexler, J. W., Jr.; Schreiner, A. F.; Cotton, F. A. *Inorg. Chem.* **1988**, *27*, 3265−3267. (b) Boyar, E. B.; Robinson, S. D. *Coord. Chem. Rev.* **1983**, *50*, 109−208. (c) Sowa, T.; Kawamura, T.; Shida, T.; Yonezawa, T. *Inorg. Chem.* **1983**, *22*, 56−61. (d) Felthouse, T. R. *Prog. Inorg. Chem.* **1982**, *29*, 73−166. (e) Martin, D. S., Jr.; Webb, T. R.; Robbins, G. A.; Fanwick, P. E. *Inorg. Chem.* **1979**, *18*, 475−478. (f) Norman, J. G., Jr.; Kolari, H. J. *J. Am. Chem. Soc.* **1978**, *100*, 791−799. (g) Dubicki, L.; Martin, R. L. *Inorg. Chem.* **1970**, *9*, 673−675.
(46) Zhu, T. P.; Ahsan, M. Q.; Malinski, T.; Kadish, K. M.; Bear, J. L. *Inorg. Chem.* **1984**, *23*, 2−3.